

REFLECTION AND TRANSMISSION OF AN ELECTROMAGNETIC X-WAVE INCIDENT ON A PLANAR AIR-DIELECTRIC INTERFACE: SPECTRAL ANALYSIS

A. M. Shaarawi[†]

Physics Department
The American University in Cairo
P.O. Box 2511, Cairo 11511, Egypt

I. M. Besieris

The Bradley Department of Electrical and Computer Engineering
Virginia Polytechnic Institute and State University
Blacksburg, Virginia 24061, USA

A. M. Attiya and E. El-Diwany

Department of Microwave Engineering
Electronic Research Institute, Dokki
Giza, 12211, Egypt

Abstract—The spectral structure of the reflected and transmitted fields due to a three dimensional electromagnetic X-wave incident on a planar air-dielectric interface is examined. Using a novel superposition of azimuthally dependent pulsed plane waves, it is shown that for oblique incidence the reflected pulse has a localized wave structure. On the other hand, the transmitted field maintains its localization up to a certain distance from the interface beyond which it starts disintegrating. A study of the effects of polarization on the amplitudes of the reflected and transmitted wave fields is presented.

[†] Permanent address: Department of Engineering Physics and Mathematics, Faculty of Engineering, Cairo University, Giza 12211, Egypt.

1. Introduction
 2. The Spectral Composition of the Incident, Reflected and Transmitted Fields
 - 2.1 Spectral Composition of a Normally Incident TE Electromagnetic X-wave
 - 2.2 The Obliquely Incident TE X-wave
 - 2.3 The Reflected and Transmitted Wave Fields
 - 2.4 The Transmitted Electric Field Intensity for Normal Incidence
 3. Numerical Examples
 4. Conclusion
- Appendices
References

1. INTRODUCTION

Recently, it has been realized that two classes of ultra-wide-band pulses, specifically wave solutions based on focus wave modes [1–3] and X-waves [4–6], have similar spectral attributes. As such, we regard these two groups of pulsed waves as subdivisions of a larger class of solutions; namely, localized waves (LW) [7, 8]. Localized waves have been studied extensively during the past decade. Schemes to generate acoustical and optical LWs have been proposed and tested experimentally [9–11]. Furthermore, investigations concerned with their use in high-resolution imaging [12] and target identification [13] have demonstrated certain advantages for LWs over other pulses. Because of their large focusing depths and ultra-wide-band spectra, LWs offer greater utility in detecting objects buried at different depths and in identifying wide ranges of parameters characterizing detected targets [13]. In such applications, one expects electromagnetic localized waves to be transmitted from one medium to another. It is, therefore, important to study the details of a canonical problem involving the reflection and transmission of a localized wave obliquely incident on a planar interface separating two electrically different materials. This problem has been investigated previously in three different papers [14–16]. In the first two studies, the authors used a two-dimensional variation of Brittingham’s FWM solution. Hillion argued that FWMs are only transmitted across a discontinuity surface if they are normally incident on that surface, while for oblique incidence only reflection takes place [14]. Furthermore, he demonstrated that for normal incidence

the transmitted, reflected and incident fields have LW structures. Donnelly and Power, on the other hand, proved that for oblique incidence the reflected waveform has a LW structure while the transmitted field does not [15]. In the third paper, the authors investigated the case of a three-dimensional acoustical X-wave. They demonstrated that the transmitted field loses its LW structure; however, it stays localized for a certain distance before it starts disintegrating [16]. Furthermore, they were able to deduce an expression for the dispersion-free range and confirm numerically that such an estimate is consistent with the decay pattern of the transmitted field.

In this work, we extend our previous study to the case of a three-dimensional electromagnetic X-wave incident on an interface separating two electrically different media. We show that for oblique incidence the reflected X-wave has a LW structure. We also provide an explanation for the dispersion of the transmitted field. This explanation is based on a spectral analysis that leads to a representation involving an integration of an angular distribution of azimuthally dependent elementary pulses. For the incident and reflected X-waves, all the azimuthally dependent pulses travel at the same speed and add up coherently at any observation point to synthesize a diffraction-free LW pulse. In contradistinction, the transmitted azimuthally dependent pulses travel at different speeds. The integration of these dispersed pulses results in a wave field having an axial width that increases with distance from the interface. This causes the central part of the transmitted pulse to become longer, and the amplitude of its peak to decrease with distance. This idea is consistent with the ray-theoretic explanation provided in Ref. 17.

The incident LW pulse is chosen to be a three-dimensional X-wave because it is mathematically easier to manipulate than a three-dimensional FWM pulse. This is the case because the wave vectors of the X-wave lie on a conic surface whose apex angle is a parameter appearing explicitly in the mathematical expression representing the X-wave solution [17–19]. On the other hand, the components of the FWM field form a weighted distribution over an infinite number of uniaxial cones [20]. The apex angles can take any values between 0 to π ; therefore, acausal incoming components contribute to the total field. Causally, it is necessary to deal with fields traveling only in one direction. In previous studies, it has been shown how to choose the parameters entering into the FWM solution in order to construct a LW

field whose components are mostly traveling from one hemisphere to the other [3, 20, 21]. This is achieved by tweaking the parameters appearing in the FWM solution so that the wave vectors defined on cones having angles $\pi/2$ to π have larger spectral amplitudes (weights) than those having angles 0 to $\pi/2$. The latter acausal components become negligible and can be eliminated without affecting the shape or the localized character of the propagating wave. In the interface problem, one has always to keep track of a basic fact; namely, the identification of the side of the separating surface from which the wave components are incident. This becomes a crucial issue for an obliquely incident FWM pulse because the common axis of the cones, on which the wave vectors are distributed, is tilted with respect to the normal to the separating surface. Thus, we should be watchful for the possibility of having components of relatively large spectral amplitudes arriving from the lower side of the interface. This is a senseless situation and can be a source of great confusion and can lead to incorrect conclusions.

The plan of this work is to deduce spectral superpositions representing the reflected and transmitted fields resulting from an X-wave incident on an air-dielectric interface. This is done in Sec. 2. Starting with the Fourier composition of the incident X-wave, the corresponding Fourier superpositions of the reflected and transmitted fields are deduced. The resulting expressions for the various field components are then transformed into angular superpositions over azimuthally dependent pulses. The latter are used in evaluating numerically the different field components and determining the polarization of the transmitted field. Numerical calculations are discussed in Sec. 3, where it is shown that the reflected field does not lose its LW properties, while the transmitted field does. Factors affecting the disintegration of the transmitted pulse are identified and their effect on the dispersion-free range of the transmitted field is pointed out. In Sec. 4, we provide concluding remarks and discuss possible future developments.

2. THE SPECTRAL COMPOSITION OF THE INCIDENT, REFLECTED AND TRANSMITTED FIELDS

The X-wave field is composed of plane waves characterized by wave vectors lying on a conical surface defined in momentum space by the apex angle $\theta_k = \xi$ [17–19]. For oblique incidence, the spectral cone [cf. Fig. 1 in Ref. 17] must be rotated by an angle equal to the angle of incidence. Following a procedure introduced for acoustical X-waves

incident on a discontinuity surface [16], we transform the Fourier spectral superposition of the electromagnetic X-wave into an azimuthally dependent angular representation [cf. Eq. (11) in Ref. 17]. Such an azimuthal angular superposition has proved to be very effective in calculating the amplitudes of the reflected and transmitted acoustical fields [16].

2.1 Spectral Composition of a Normally Incident TE Electromagnetic X-wave

Consider a TE electromagnetic X-wave traveling in the positive z -direction incident normally at the interface ($z = 0$) separating two electrically distinct media. In particular, we assume that the normally incident field is circularly polarized, i.e., the electric field component is in the direction of the vector \vec{u}_ϕ . A spatio-temporal representation of such a field can be written as a four-fold Fourier superposition, viz.,

$$\vec{E}(\vec{r}, t) = \int_0^\infty d(\omega/c_1) \int_{R^3} d^3\vec{k} e^{i\omega t} e^{-i\vec{k}\cdot\vec{r}} \vec{E}_\phi(\vec{k}, \omega/c_1) \vec{u}_\phi(\vec{k}, (\omega/c_1)) \cdot \delta(k_x^2 + k_y^2 + k_z^2 - (\omega/c_1)^2), \quad (1)$$

where c_1 denotes the phase speed of electromagnetic waves in the region $z < 0$ and

$$\vec{E}_\phi(\vec{k}, (\omega/c_1)) = A(\vec{k}, (\omega/c_1)) / \pi, \quad \vec{u}_\phi = ((-k_y/\chi)\vec{u}_x + (k_x/\chi)\vec{u}_y), \\ \chi = \sqrt{k_x^2 + k_y^2}.$$

In this work, we choose the real part of the complex integration given in Eq. (1) to represent the electric field. This choice applies to the incident, reflected and transmitted fields. To obtain an X-wave-type solution, we choose:

$$A(\vec{k}, (\omega/c_1)) = F(\vec{k}, (\omega/c_1)) \delta(k_z - (\omega/c_1) \cos \xi), \quad 0 \leq \xi < \pi/2.$$

It follows, then, that

$$\vec{E}(\vec{r}, t) = (1/\pi) \int_0^\infty d(\omega/c_1) \int_{R^3} d^3\vec{k} e^{i\omega t} e^{-i\vec{k}\cdot\vec{r}} F(\vec{k}, (\omega/c_1)) \cdot \delta(k_z - (\omega/c_1) \cos \xi) (-k_y/\chi)\vec{u}_x + (k_x/\chi)\vec{u}_y \cdot \delta(k_x^2 + k_y^2 + k_z^2 - (\omega/c_1)^2). \quad (2)$$

We introduce, next, polar coordinates in wavenumber space by means of the relations $k_x = \chi \cos \phi$ and $k_y = \chi \sin \phi$. After integrating over k_z , Eq. (2) assumes the form

$$\vec{E}(x, y, z, t) = (1/\pi) \int_0^\infty d(\omega/c_1) \int_0^{2\pi} d\phi \int_0^\infty d\chi \chi e^{i\omega t} e^{-i(\chi x \cos \phi)} e^{-i(\chi y \sin \phi)} \cdot e^{-i(\omega/c_1)z \cos \xi} F((\omega/c_1), \chi, \phi) \vec{s}_e(\phi) \delta(\chi^2 - (\omega/c_1)^2 \sin^2 \xi), \quad (3)$$

where

$$\vec{s}_e(\phi) = (-\sin \phi \vec{u}_x + \cos \phi \vec{u}_y).$$

Integrating over χ , we obtain

$$\vec{E}(x, y, z, t) = (1/2\pi) \int_0^\infty d(\omega/c_1) \int_0^{2\pi} d\phi e^{i\omega t} e^{-i(\omega/c_1) \sin \xi (x \cos \phi + y \sin \phi)} \cdot e^{-i(\omega/c_1)z \cos \xi} \tilde{F}((\omega/c_1), \phi) \vec{s}_e(\phi). \quad (4)$$

Choosing

$$\tilde{F}((\omega/c_1), \phi) = ie^{-(\omega/c_1)a} f(\phi), \quad a > 0, \quad (5)$$

we get

$$\vec{E}(x, y, z, t) = (i/2\pi) \int_0^{2\pi} d\phi \int_0^\infty d(\omega/c_1) e^{-i(\omega/c_1)(z \cos \xi - c_1 t)} \cdot e^{-i(\omega/c_1) \sin \xi (x \cos \phi + y \sin \phi)} e^{-(\omega/c_1)a} f(\phi) \vec{s}_e(\phi).$$

The integration over (ω/c) results in the expression

$$\vec{E}(x, y, z, t) = \frac{i}{2\pi} \int_0^{2\pi} d\phi \frac{f(\phi) \vec{s}_e(\phi)}{(a + i(z \cos \xi - c_1 t) + i \sin \xi (x \cos \phi + y \sin \phi))}. \quad (6)$$

It is clear that the choice of $f(\phi)$ affects the polarization of the resulting field. The simplest expression follows from choosing $f(\phi) = 1$. A scalar-valued version of the azimuthal angular superposition given in Eq. (6) has been used previously to determine the properties of the reflected and transmitted fields due to an acoustic X-wave incident on a surface of discontinuity separating two media [16].

An azimuthal angular superposition for the magnetic field intensity can be obtained in an analogous fashion. It is given explicitly as follows:

$$\vec{H}(x, y, z, t) = \frac{i}{2\pi} \sqrt{\frac{\varepsilon_r \varepsilon_0}{\mu_0}} \int_0^{2\pi} d\phi \times \frac{f(\phi) \{\vec{\gamma}(\phi) \times \vec{s}_e(\phi)\}}{(a + i(z \cos \xi - c_1 t) + i \sin \xi (x \cos \phi + y \sin \phi))}. \quad (7)$$

Here $c_1 = (c_0/\sqrt{\varepsilon_r})$, where c_0 denotes the speed of light in vacuum and ε_r the relative permittivity of the medium in region $z < 0$ and the magnetic permeability is assumed to be that of vacuum. The ϕ -dependent unit vector associated with each propagation vector \vec{k} is denoted by $\vec{\gamma}(\phi)$ [cf. Appendix B]. For normal incidence, we have

$$\vec{\gamma}_i(\phi) = \sin \xi \cos \phi \vec{u}_x + \sin \xi \sin \phi \vec{u}_y + \cos \xi \vec{u}_z.$$

In this case, the magnetic field intensity given in Eq. (7) simplifies to

$$\begin{aligned} \vec{H}(x, y, z, t) = & \frac{i}{2\pi} \sqrt{\frac{\varepsilon_r \varepsilon_0}{\mu_0}} \int_0^{2\pi} d\phi \\ & \times \frac{f(\phi) \vec{s}_h(\phi)}{(a + i(z \cos \xi - c_1 t) + i \sin \xi (x \cos \phi + y \sin \phi))}. \end{aligned} \quad (8)$$

where

$$\vec{s}_h(\phi) = \sin \xi \vec{u}_z - \cos \xi (\cos \phi \vec{u}_x + \sin \phi \vec{u}_y).$$

It is seen from this expression that the magnetic field $\vec{H}(\vec{r}, t)$ has a transverse component parallel to the surface of discontinuity given by

$$\begin{aligned} \vec{H}_\perp(x, y, z, t) = & -\frac{i}{2\pi} \sqrt{\frac{\varepsilon_r \varepsilon_0}{\mu_0}} \int_0^{2\pi} d\phi f(\phi) \\ & \times \frac{\cos \xi (\cos \phi \vec{u}_x + \sin \phi \vec{u}_y)}{(a + i(z \cos \xi - c_1 t) + i \sin \xi (x \cos \phi + y \sin \phi))}, \end{aligned} \quad (9a)$$

and a longitudinal component normal to the surface of discontinuity given as

$$\begin{aligned} \vec{H}_\parallel(x, y, z, t) = & \frac{i}{2\pi} \sqrt{\frac{\varepsilon_r \varepsilon_0}{\mu_0}} \int_0^{2\pi} d\phi f(\phi) \\ & \times \frac{\sin \xi \vec{u}_z}{(a + i(z \cos \xi - c_1 t) + i \sin \xi (x \cos \phi + y \sin \phi))}. \end{aligned} \quad (9b)$$

In the following subsections, we shall deal only with the electric field components bearing in mind that the magnetic components can be calculated using the procedure described in the preceding paragraphs.

The space-time dependence of the electromagnetic field components in Eqs. (6) and (9a, b) is determined by the kernel

$$K(x, y, z, t; \phi) = (a + i(z \cos \xi - c_1 t) + i \sin \xi (x \cos \phi + y \sin \phi))^{-1} \quad (10)$$

that appears in the integrands of the three expressions. This kernel represents various azimuthally dependent pulses arriving simultaneously at a certain point, thus contributing coherently to the amplitude of a nondispersive X-shaped LW. One can, thus, conjecture that the existence of such kernel (or similar ones resulting from simple coordinate rotations) implies that the field has a nondispersive LW structure. This could be a useful measure in determining whether the reflected and transmitted fields retain the LW character of the incident X-wave.

2.2 The Obliquely Incident TE X-Wave

For an obliquely incident X-wave, having its axis of propagation tilted at an angle α_1 to the z -axis (the normal to the interface), the \vec{k} and \vec{s} vectors should be rotated as specified in Appendix A. Consequently, the electric field intensity acquires the form

$$\vec{E}^{(i)}(\vec{r}, t) = (i/2\pi) \int_0^\infty d(\omega/c_1) \cdot \int_0^{2\pi} d\phi e^{i\omega t} e^{-i(k'_x x + k'_y y + k'_z z)} f(\phi) e^{-(\omega/c_1)a \vec{s}^{(i)}}, \quad (11)$$

where

$$\vec{s}^{(i)} = \frac{1}{\sqrt{k'_x{}^2 + (k'_y \cos \alpha_1 + k'_z \sin \alpha_1)^2}} \cdot \{ - (k'_y \cos \alpha_1 + k'_z \sin \alpha_1) \vec{u}_x + k'_x \cos \alpha_1 \vec{u}_y + k'_x \sin \alpha_1 \vec{u}_z \}. \quad (12)$$

The wave vector components associated with the obliquely incident X-wave, viz., $(k'_x, k'_y, k'_z) = (k_{xinc}, k_{yinc}, k_{zinc})$ are given in Eqs. (B1–3) of Appendix B. The substitution of the above expressions for k'_x, k'_y and k'_z into (12) yields an alternative expression for $\vec{s}^{(i)}$ which depends solely on the angular variables; specifically,

$$\vec{s}^{(i)} = -\sin \phi \vec{u}_x + \sin \phi \cos \alpha_1 \vec{u}_y + \cos \phi \sin \alpha_1 \vec{u}_z. \quad (13)$$

It is important to note that the polarization vector $\vec{s}^{(i)}$ is independent of (ω/c_1) . The integration over (ω/c_1) in Eq. (11) can be easily evaluated yielding

$$\vec{E}^{(i)}(\vec{r}, t) = \frac{i}{2\pi} \int_0^{2\pi} d\phi \times \frac{f(\phi) (-\sin \phi \vec{u}_x + \cos \phi \cos \alpha_1 \vec{u}_y + \cos \phi \sin \alpha_1 \vec{u}_z)}{\left(a + i((z \cos \alpha_1 - y \sin \alpha_1) \cos \xi_1 - c_1 t) + ix \sin \xi_1 \cos \phi + i \sin \xi_1 \sin \phi (y \cos \alpha_1 + z \sin \alpha_1) \right)}. \quad (14)$$

The fact that the polarization vector is independent of (ω/c_1) greatly simplifies our analysis. In later sections, we shall use the same property to calculate the reflected and transmitted coefficients given that the Fresnel coefficients of the reflected and transmitted fields are also independent of (ω/c_1) . To calculate the reflected and transmitted fields, the obliquely incident X-wave should be split into spectral components that are parallel and normal to the plane of incidence. This requires Eq. (14) to be rewritten in a different fashion. Specifically, the integration in Eq. (14) should be divided into two parts, viz.,

$$\vec{E}^{(i)}(\vec{r}, t) = \frac{i}{2\pi} \int_0^{2\pi} d\phi f(\phi) K^{(i)}(x, y, z, t; \phi) \vec{s}_\perp^{(i)}(\phi) + \frac{i}{2\pi} \int_0^{2\pi} d\phi f(\phi) K^{(i)}(x, y, z, t; \phi) \vec{s}_\parallel^{(i)}(\phi), \quad (15)$$

where the kernel of the obliquely incident field is given as

$$K^{(i)}(x, y, z, t; \phi) = (a + i((z \cos \alpha_1 - y \sin \alpha_1) \cos \xi_1 - c_1 t) + ix \sin \xi_1 \cos \phi + i \sin \xi_1 \sin \phi (y \cos \alpha_1 + z \sin \alpha_1))^{-1}. \quad (16)$$

The procedure described in Appendix A gives the parallel and normal components of the polarization vector. Substituting the components of the wave vector $(k'_x, k'_y, k'_z) = (k_{xinc}, k_{yinc}, k_{zinc})$ given in Eqs. (B1–3), we have

$$\vec{s}_\perp^{(i)} = \frac{\gamma_y (\gamma_y \cos \alpha_1 + \gamma_z \sin \alpha_1) + \gamma_x^2 \cos \alpha_1}{(\gamma_x^2 + \gamma_y^2) \sqrt{\gamma_x^2 + (\gamma_y \cos \alpha_1 + \gamma_z \sin \alpha_1)^2}} \{-\gamma_y \vec{u}_x + \gamma_x \vec{u}_y\}. \quad (17a)$$

$$\vec{s}_\parallel^{(i)} = \frac{\gamma_x \sin \alpha_1}{\sqrt{\gamma_x^2 + (\gamma_y \cos \alpha_1 + \gamma_z \sin \alpha_1)^2}} \left\{ \frac{-\gamma_z}{(\gamma_x^2 + \gamma_y^2)} (\gamma_x \vec{u}_x + \gamma_y \vec{u}_y) + \vec{u}_z \right\}. \quad (17b)$$

Using Eq. (15), the obliquely incident magnetic field intensity can be calculated as follows

$$\begin{aligned} \vec{H}^{(i)}(\vec{r}, t) &= \frac{i}{2\pi} \sqrt{\frac{\varepsilon_1 \varepsilon_0}{\mu_0}} \int_0^{2\pi} d\phi f(\phi) K^{(i)}(x, y, z, t; \phi) \left\{ \vec{\gamma}(\phi) \times \vec{s}_{\perp}^{(i)}(\phi) \right\} \\ &+ \frac{i}{2\pi} \sqrt{\frac{\varepsilon_1 \varepsilon_0}{\mu_0}} \int_0^{2\pi} d\phi f(\phi) K^{(i)}(x, y, z, t; \phi) \left\{ \vec{\gamma}(\phi) \times \vec{s}_{\parallel}^{(i)}(\phi) \right\}. \end{aligned} \quad (18)$$

2.3 The Reflected and Transmitted Wave Fields

To evaluate the reflected and transmitted field components, one can apply the Fresnel formulas for the electric field [22], viz.,

$$R_{\parallel} = \frac{\eta_1 \cos \theta_{k1} - \eta_2 \cos \theta_{k2}}{\eta_1 \cos \theta_{k1} + \eta_2 \cos \theta_{k2}}, \quad (19a)$$

$$R_{\perp} = \frac{\eta_2 \cos \theta_{k1} - \eta_1 \cos \theta_{k2}}{\eta_2 \cos \theta_{k1} + \eta_1 \cos \theta_{k2}}. \quad (19b)$$

$$T_{\parallel} = \frac{2\eta_2 \cos \theta_{k1}}{\eta_1 \cos \theta_{k1} + \eta_2 \cos \theta_{k2}}, \quad (20a)$$

$$T_{\perp} = \frac{2\eta_2 \cos \theta_{k1}}{\eta_2 \cos \theta_{k1} + \eta_1 \cos \theta_{k2}}. \quad (20b)$$

Here, $\eta_1 = \sqrt{\mu_0 \mu_1 / \varepsilon_0 \varepsilon_1}$ and $\eta_2 = \sqrt{\varepsilon_0 \varepsilon_2 / \mu_0 \mu_2}$ are the intrinsic impedances of the two media. The spectral angles θ_{k1} and θ_{k2} can be evaluated using Eq. (18a) in Ref. 17. Using the notation introduced in Appendix B, we have

$$\gamma_z(\phi) = \cos \theta_{k1} = \sin \xi_1 \sin \alpha_1 \sin \phi + \cos \xi_1 \cos \alpha$$

and

$$\begin{aligned} \tilde{\gamma}_z(\phi) &= (c_1/c_2) \cos \theta_{k2} \\ &= (c_1/c_2) \sqrt{1 - (c_2/c_1)^2 + (c_2/c_1)^2 (\sin \xi_1 \sin \alpha_1 \sin \phi + \cos \xi_1 \cos \alpha)^2}. \end{aligned}$$

The Fresnel formulas for nonmagnetic media acquire the following angular dependent forms

$$R_{\parallel}(\phi) = \frac{\gamma_z(\phi) - (c_2/c_1)^2 \tilde{\gamma}_z(\phi)}{\gamma_z(\phi) + (c_2/c_1)^2 \tilde{\gamma}_z(\phi)}, \quad (21a)$$

$$R_{\perp}(\phi) = \frac{\gamma_z(\phi) - \tilde{\gamma}_z(\phi)}{\gamma_z(\phi) + \tilde{\gamma}_z(\phi)}. \quad (21b)$$

$$T_{\parallel}(\phi) = \frac{2(c_2/c_1)\gamma_z(\phi)}{\gamma_z(\phi) + (c_2/c_1)^2\tilde{\gamma}_z(\phi)}, \quad (22a)$$

$$T_{\perp}(\phi) = \frac{2\gamma_z(\phi)}{\gamma_z(\phi) + \tilde{\gamma}_z(\phi)}. \quad (22b)$$

To calculate the reflected field, we need to determine the reflected spectral amplitude for each azimuthal pulsed component. Multiplying the electric field components (normal and parallel to the plane of incidence) by the appropriate Fresnel coefficients yields

$$\begin{aligned} \vec{E}^{(r)}(\vec{r}, t) &= \frac{i}{2\pi} \int_0^{2\pi} d\phi f(\phi) K^{(r)}(x, y, z, t; \phi) \vec{s}_{\perp}^{(r)}(\phi) R_{\perp}(\phi) \\ &+ \frac{i}{2\pi} \int_0^{2\pi} d\phi f(\phi) K^{(r)}(x, y, z, t; \phi) \vec{s}_{\parallel}^{(r)}(\phi) R_{\parallel}(\phi), \end{aligned} \quad (23)$$

where the kernel of the reflected field, viz.,

$$\begin{aligned} K^{(r)}(x, y, z, t; \phi) &= (a - i((z \cos \alpha_1 + y \sin \alpha_1) \cos \xi_1 + c_1 t) \\ &+ ix \sin \xi_1 \cos \phi + i \sin \xi_1 \sin \phi (y \cos \alpha_1 - z \sin \alpha_1))^{-1} \end{aligned} \quad (24)$$

follows from an integration over (ω/c_1) in an expression analogous to that in Eq. (11). For the reflected field one has to substitute $(k'_x, k'_y, k'_z) = (k_{xref}, k_{yref}, k_{zref})$ given in Eqs. (B4–6). The parallel and normal components of the polarization vector of the reflected electric field intensity are deduced using Eqs. (A11–12) and (B4–6). They are given explicitly as follows:

$$\vec{s}_{\perp}^{(r)} = \frac{\gamma_y(-\gamma_y \cos \alpha_1 - \gamma_z \sin \alpha_1) - \gamma_x^2 \cos \alpha_1}{(\gamma_x^2 + \gamma_y^2) \sqrt{\gamma_x^2 + (-\gamma_y \cos \alpha_1 - \gamma_z \sin \alpha_1)^2}} \{-\gamma_y \vec{u}_x + \gamma_x \vec{u}_y\}, \quad (25)$$

$$\vec{s}_{\parallel}^{(r)} = \frac{\gamma_x \sin \alpha_1}{\sqrt{\gamma_x^2 + (-\gamma_y \cos \alpha_1 - \gamma_z \sin \alpha_1)^2}} \left\{ \frac{\gamma_z}{(\gamma_x^2 + \gamma_y^2)} (\gamma_x \vec{u}_x + \gamma_y \vec{u}_y) + \vec{u}_z \right\}. \quad (26)$$

In these two expressions, we have applied $\cos \alpha_1 \rightarrow -\cos \alpha_1$ ($\cos(\pi - \alpha_1) = -\cos \alpha_1$) and $\sin(\pi - \alpha_1) = \sin \alpha_1$) to the expressions given in

(A11) and (A12). As discussed in Appendix B, such a transformation is necessary for constructing a reflected cone satisfying the reflection condition $\theta_{k1} = \theta_{k2}$.

The reflected magnetic field intensity can be calculated from Eq. (23). It assumes the following angular superposition form:

$$\begin{aligned} \vec{H}^{(r)}(\vec{r}, t) = & \frac{i}{2\pi} \sqrt{\frac{\varepsilon_1 \varepsilon_0}{\mu_0}} \int_0^{2\pi} d\phi f(\phi) K^{(r)}(x, y, z, t; \phi) \left\{ \vec{\gamma}(\phi) \times \vec{s}_{\perp}^{(r)}(\phi) \right\} R_{\perp}(\phi) \\ & + \frac{i}{2\pi} \sqrt{\frac{\varepsilon_1 \varepsilon_0}{\mu_0}} \int_0^{2\pi} d\phi f(\phi) K^{(r)}(x, y, z, t; \phi) \left\{ \vec{\gamma}(\phi) \times \vec{s}_{\parallel}^{(r)}(\phi) \right\} R_{\parallel}(\phi). \end{aligned} \quad (27)$$

The transmitted electric field intensity is calculated by applying a similar procedure. Starting with the parallel and perpendicular components of the incident field, we multiply the azimuthal angular components by the appropriate Fresnel coefficient and substitute the expressions for $k'_z = k_{ztrans}$, $k'_y = k_{ytrans}$, and $k'_x = k_{xtrans}$ given in Appendix B. The resulting transmitted electric field is equal to

$$\begin{aligned} \vec{E}^{(t)}(\vec{r}, t) = & \frac{i}{2\pi} \int_0^{2\pi} d\phi f(\phi) K^{(t)}(x, y, z, t; \phi) \vec{s}_{\perp}^{(t)}(\phi) T_{\perp}(\phi) \\ & + \frac{i}{2\pi} \int_0^{2\pi} d\phi f(\phi) K^{(t)}(x, y, z, t; \phi) \vec{s}_{\parallel}^{(t)}(\phi) T_{\parallel}(\phi). \end{aligned} \quad (28)$$

Here, the kernel of the transmitted field is deduced by carrying out Fourier integrations appearing in an expression analogous to Eq. (11). The function $K^{(t)}(x, y, z, t; \phi)$ resulting from the integration over (ω/c_1) is given as

$$K^{(t)}(x, y, z, t; \phi) = (a + i(z\tilde{\gamma}_z(\phi) - c_1 t) + ix \sin \xi_1 \cos \phi + iy\gamma_y(\phi))^{-1}. \quad (29)$$

In Appendix A, Eqs. (A11) and (A12) give the parallel and normal parts of the polarization vector for the transmitted field. Substituting the components of the wave vector $(k'_x, k'_y, k'_z) = (k_{xinc}, k_{yinc}, k_{zinc})$ given in Eqs. (B7, 8) and (B12), we obtain

$$\vec{s}_{\perp}^{(t)} = \frac{\gamma_y(\gamma_y \cos \alpha_1 + \tilde{\gamma}_z \sin \alpha_1) + \gamma_x^2 \cos \alpha_1}{(\gamma_x^2 + \gamma_y^2) \sqrt{\gamma_x^2 + (\gamma_y \cos \alpha_1 + \tilde{\gamma}_z \sin \alpha_1)^2}} \{-\gamma_y \vec{u}_x + \gamma_x \vec{u}_y\}, \quad (30a)$$

$$\vec{s}_{\parallel}^{(t)} = \frac{\gamma_x \sin \alpha_1}{\sqrt{\gamma_x^2 + (\gamma_y \cos \alpha_1 + \tilde{\gamma}_z \sin \alpha_1)^2}} \left\{ \frac{-\tilde{\gamma}_z}{(\gamma_x^2 + \gamma_y^2)} (\gamma_x \vec{u}_x + \gamma_y \vec{u}_y) + \vec{u}_z \right\}. \quad (30b)$$

The transmitted magnetic field intensity can be calculated using the following angular superposition:

$$\begin{aligned} \vec{H}^{(t)}(\vec{r}, t) &= \frac{i}{2\pi} \sqrt{\frac{\varepsilon_2 \varepsilon_0}{\mu_0}} \int_0^{2\pi} d\phi f(\phi) K^{(t)}(x, y, z, t; \phi) \left\{ \vec{\gamma}(\phi) \times \vec{s}_{\perp}^{(t)}(\phi) \right\} T_{\perp}(\phi) \\ &+ \frac{i}{2\pi} \sqrt{\frac{\varepsilon_2 \varepsilon_0}{\mu_0}} \int_0^{2\pi} d\phi f(\phi) K^{(t)}(x, y, z, t; \phi) \left\{ \vec{\gamma}(\phi) \times \vec{s}_{\parallel}^{(t)}(\phi) \right\} T_{\parallel}(\phi). \end{aligned} \quad (31)$$

Notice that in Eqs. (29–31), the space and time dependence of the transmitted field is due to an angular integration of a kernel that differs from the one given in Eq. (10). The z -components of the velocities of the azimuthal pulses depend on the angular variable ϕ . The various pulsed components traveling with different velocities cause the transmitted field to disperse. Once it goes through the interface, the transmitted field is initially localized. When the dispersion of the pulsed components spans a distance comparable to $a' = a(c_2/c_1)/\cos \xi_2$ the transmitted pulse starts disintegrating. Consequently, pulses having large a values or small ξ_2 angles propagate for longer distances before they start dispersing. These results have been confirmed numerically for acoustic X-waves [16] and will be examined in the next section for electromagnetic X-waves.

2.4 The Transmitted Electric Field Intensity for Normal Incidence

Before considering specific numerical examples, we examine the case of normal incidence for which $\alpha_1 = 0$. In this limit the quantity $\tilde{\gamma}_z(\phi)$ reduces to $(c_1/c_2) \cos \xi_2$. As a consequence, the transmitted electric field given in Eq. (28) reduces to

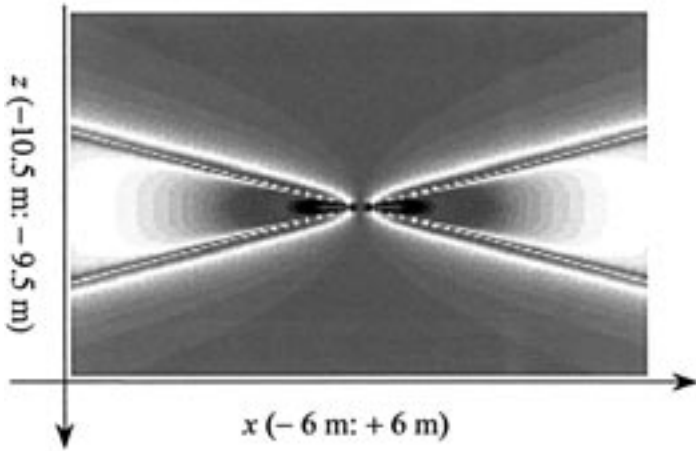
$$\begin{aligned} \vec{E}^{(t)}(x, y, z, t) &= \frac{i}{2\pi} \int_0^{2\pi} d\phi \\ &\times \frac{(c_2/c_1) f(\phi) (-\sin \phi \vec{u}_x + \cos \phi \vec{u}_y)}{(a(c_2/c_1) + i(z \cos \xi_2 - c_2 t) + i \sin \xi_2 (x \cos \phi + y \sin \phi))} \end{aligned}$$

$$\times \frac{2 \cos \xi_1}{\cos \xi_1 + (c_1/c_2) \cos \xi_2}. \quad (32)$$

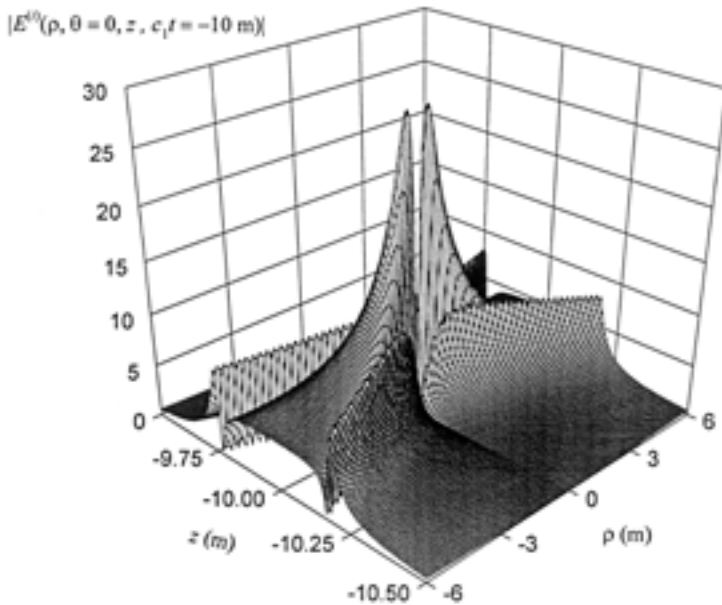
Notice that contributions from the parallel components have vanished. The integration over ϕ depends on (x, y, z, t) through a kernel similar to the one given in Eq. (10). Therefore, the transmitted field exhibits a LW structure. Its axial width along the direction of propagation equals $a' = a(c_2/c_1)/\cos \xi_2$, which is the same quantity deduced using the ray-theoretic technique used in Ref. 17. Since normally incident X-waves retain their LW structure as they are transmitted into the second medium, one expects that X-waves obliquely incident at small angles will travel for long distances without significant dispersion. It has been demonstrated that scalar X-waves incident at larger inclination angles result in transmitted fields that disperse at shorter distances. A detailed study of this behavior is considered in the next section for electromagnetic X-waves.

3. NUMERICAL EXAMPLES

In this section, we examine the behavior of the reflected and transmitted fields due to an X-wave obliquely incident on an interface separating two electrically different media. The incident TE X-wave is characterized by the parameters $\xi_1 = 2^\circ$, $a = 0.01$ m and $f(\phi) = 1$. The axis of the X-wave is inclined at an angle $\alpha_1 = 5^\circ$ relatively to the normal to the interface. The amplitude of the incident pulse is calculated at $c_1 t = -10$ m using Eqs. (15–17). Surface and density plots of the amplitude of the pulse are shown in Fig. 1 as function of the distance from the interface z and the transverse radial distance from the axis of the pulse ρ . Denoting the angular rotation in the transverse plane by ϑ we have $x = \rho \cos \vartheta$ and $y' = \rho \sin \vartheta$. Surface plots for various ϑ angles represent different sections of the pulse. The incident X-wave displayed in Fig. 1 corresponds to a section characterized by $\vartheta = 0$. Since the incident pulse introduced in Sec. 2 is rotationally invariant around the axis of propagation, we expect that its shape will not change as ϑ is varied. This can be illustrated by looking at different transverse sections evaluated at $z' \cos \xi_1 = c_1 t$. The amplitude of the electric field is plotted in Fig. 2 for different ϑ values. One can see that $|E^{(i)}(\rho, \vartheta, z' \cos \xi_1 = c_1 t)|$ evaluated at $c_1 t = -10$ m is independent of ϑ . The transverse character of the incident X-wave implies that contributions from different components to the total field vary with ϑ .



(a)



(b)

Figure 1. Magnitude of the electric field of the incident X-wave having $a = 0.01$ m and $\xi_1 = 2^\circ$ evaluated at $c_1 t = -10$ m. (a) Density plot and (b) Surface plot.

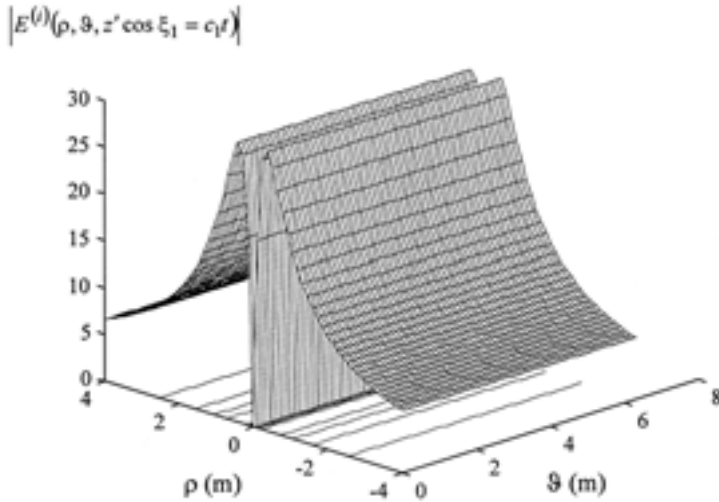
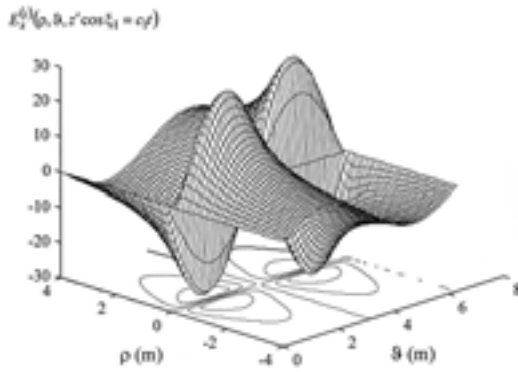


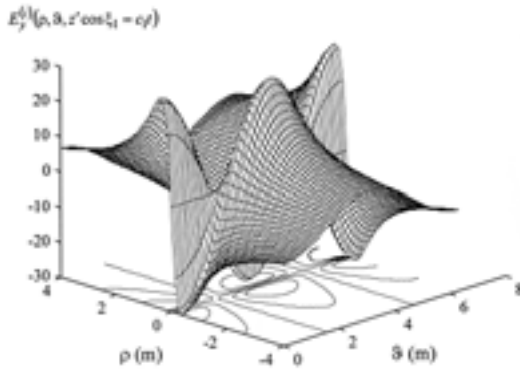
Figure 2. Surface plot of a transverse section of the incident field. The section is taken at $z' \cos \xi_1 = c_1 t = -10$ m. The incident field has $a = 0.01$ m and $\xi_1 = 2^\circ$. The amplitude is plotted as a function of ρ and ϑ .

This is illustrated in Fig. 3 by displaying the angular dependence of the three components of the incident X-wave at $z' \cos \xi_1 = c_1 t$.

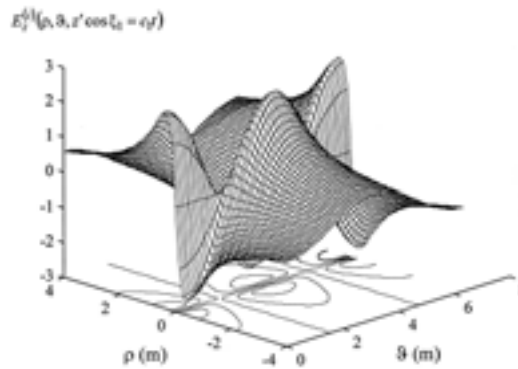
As the incident X-wave approaches the interface situated at $z = 0$, its front arms are reflected first. The peaked portion of the pulse arrives later and is reflected at an inclination angle equal to $\alpha_r = \alpha_1$. This behavior is depicted in Fig. 4 that displays a time sequence of the X-wave pulse as it approaches the interface and gets reflected. The refractive indices of the two media are chosen so that $(c_1/c_2) = 1.5$. Note that the shape of the reflected field is quite different from that of the incident one because of the varying contributions from the parallel and normal polarization components to the total field. Unlike the incident field, the reflected one is not rotationally invariant. To illustrate this point, in Fig. 5 we display density plots of sections of the reflected field at different ϑ values. Surface plots of the three sections at $\vartheta = 0, \pi/4$, and $\pi/2$ are given in Fig. 6. These figures show that the shape of the reflected field depends on the relative contribution of the normal and parallel polarization components at the various ϑ sections. To emphasize this point, in Fig. 7 we provide surface plots of the transverse reflected field at $z' \cos \xi_1 = c_1 t = 10$ m as a function



(a)



(b)



(c)

Figure 3. Surface plots of transverse sections of the three components of the incident field. The sections are taken at $z' \cos \xi_1 = c_1 t = -10$ m. The incident field has $a = 0.01$ m and $\xi_1 = 2^\circ$.

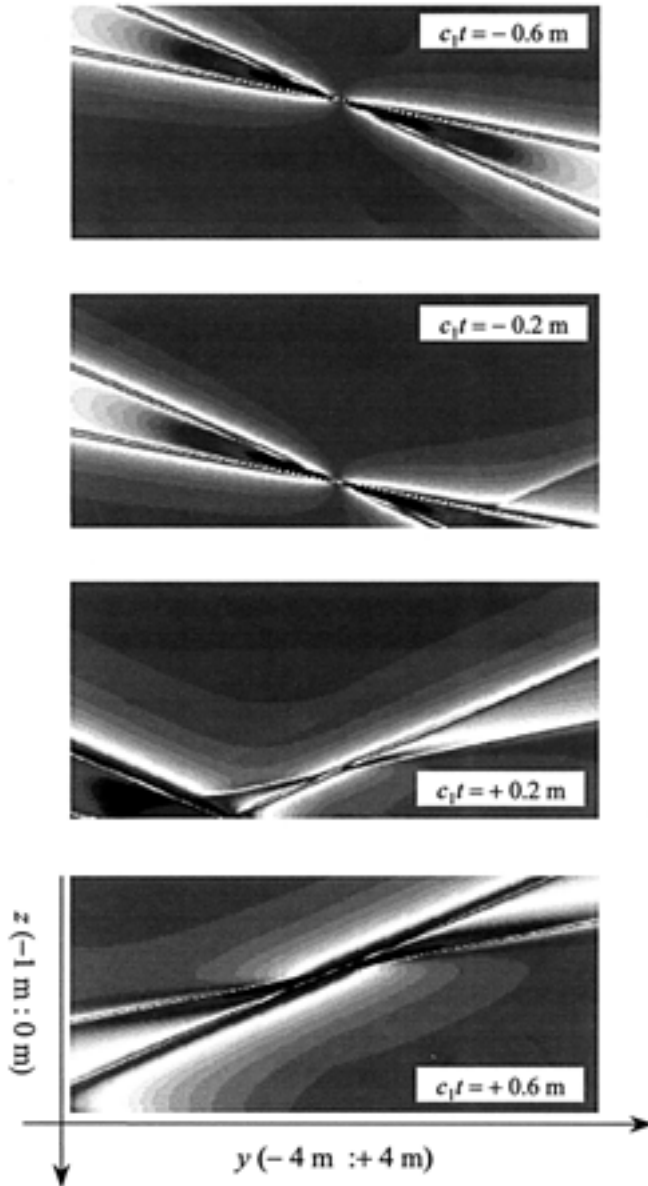


Figure 4. Density plot showing a time sequence of the incidence and reflection of the X-wave shown in Fig. 1. The dielectric medium is chosen such that $(c_1/c_2) = 1.5$ and the angle of inclination of the incident field $\alpha_1 = 5^\circ$.

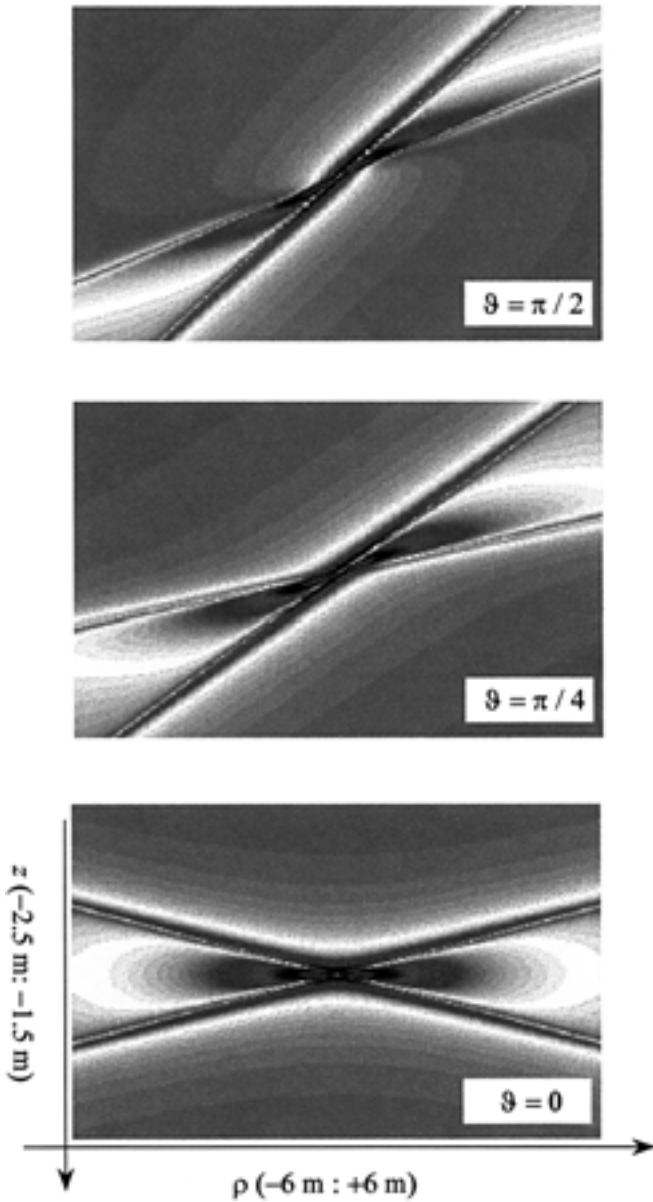
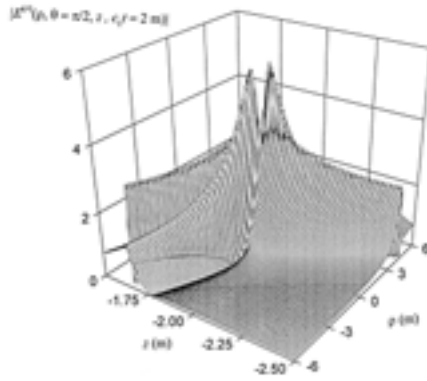
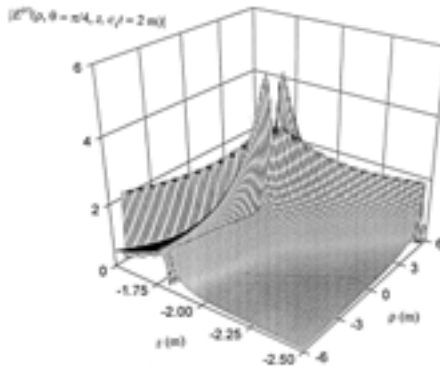


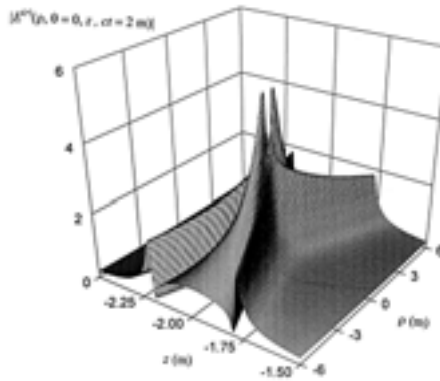
Figure 5. Density plots of the reflected electric field evaluated at $c_1 t = 10$ m for $\vartheta = 0$, $\vartheta = \pi/4$ and $\vartheta = \pi/2$. The figure illustrates the change in the shape of the reflected field evaluated at different longitudinal sections.



(a)



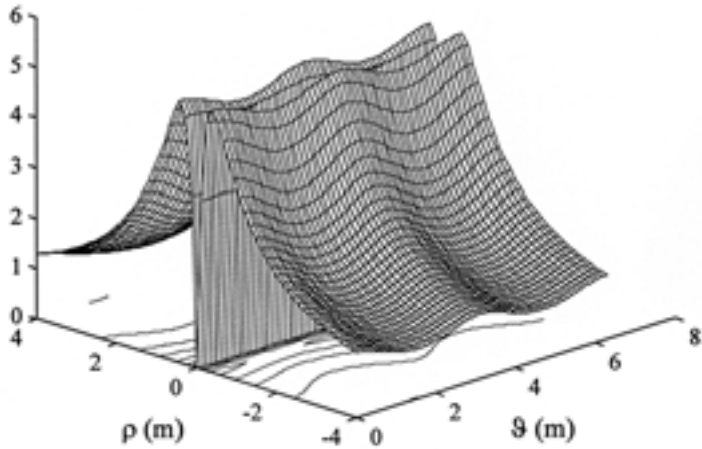
(b)



(c)

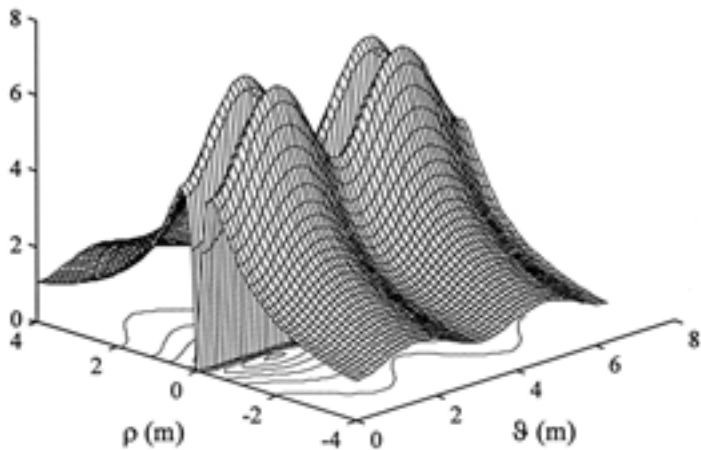
Figure 6. Surface plots of the reflected electric field evaluated at $c_1 t = 10 \text{ m}$ for (a) $\vartheta = \pi/2$, (b) $\vartheta = \pi/4$ and (c) $\vartheta = 0$.

$$|E^{(r)}(\rho, \vartheta, z' \cos \xi_1 = c_1 t)|$$



(a)

$$|E^{(r)}(\rho, \vartheta, z' \cos \xi_1 = c_1 t)|$$



(b)

Figure 7. Surface plot of a transverse section of the reflected field. The section is taken at $z' \cos \xi_1 = c_1 t = 10$ m. The incident field has $a = 0.01$ m and $\xi_1 = 2^\circ$. The amplitude is plotted as a function of ρ and ϑ for (a) $\alpha_1 = 5^\circ$ and (b) $\alpha_1 = 30^\circ$.

of ρ and ϑ . Unlike the incident field [cf. Fig. 2], the angular dependence of the amplitude of the reflected field is irregular indicating that the electric field changes significantly with ϑ . A comparison of Figs. 7a and 7b shows that the irregular dependence on ϑ becomes more pronounced as the angle of incidence is increased from $\alpha_1 = 5^\circ$ to $\alpha_1 = 30^\circ$.

Next, we consider the behavior of the transmitted field. It has been explained in Ref. [16] that the transmitted field loses its LW structure because the wave vectors defining its spectral components do not lie on a conic surface. Alternatively, one may argue that the kernel appearing in the azimuthal angular superposition given in Eqs. (28) and (29) acquires speeds that are ϕ -dependent. The transmitted field at any point inside the second medium is formed of azimuthally dependent pulses traveling at different speeds. As a result, the transmitted field disperses with distance. An estimate for the dispersion rate of the transmitted field has been deduced for acoustic X-waves [16]. The analysis introduced in that work was based on the assumption that close to the surface of discontinuity the wave vectors of the transmitted spectral components form an approximate conical surface. The inclination angle of the axis of this surface is assumed to equal α_2 and its apex angle ξ_2 . Consider the schematic diagram shown in Fig. 8. It represents a section taken at $x = 0$ of the incident, reflected and transmitted (approximate) cones. Application of Snell's law to the rays yields the following two equations:

$$(1/c_1) \sin(\alpha_1 \pm \xi_1) = (1/c_2) \sin(\alpha_2 \pm \xi_2).$$

The combination of these two equations results in the expressions

$$(1/c_1) \sin \xi_1 \cos \alpha_1 = (1/c_2) \sin \xi_2 \cos \alpha_2, \quad (33)$$

$$(1/c_1) \cos \xi_1 \sin \alpha_1 = (1/c_2) \cos \xi_2 \sin \alpha_2. \quad (34)$$

We solve for ξ_2 after eliminating the dependence on α_2 to obtain

$$\cos \xi_2 = \sqrt{-(B/2) + \sqrt{(B/2)^2 - C}}, \quad (35)$$

where $B = ((c_2/c_1)^2 \sin^2 \xi_1 \cos^2 \alpha_1 - (c_2/c_1)^2 \cos^2 \xi_1 \sin^2 \alpha_1 - 1)$ and $C = (c_2/c_1)^2 \cos^2 \xi_1 \sin^2 \alpha_1$. After evaluating the apex angle ξ_2 , the inclination angle α_2 can be calculated using either Eq. (33) or (34).

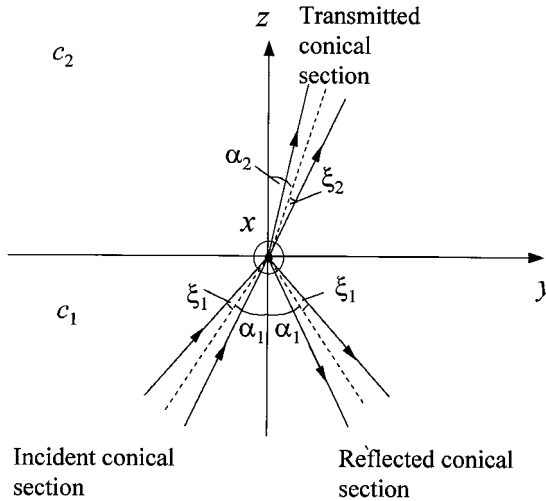


Figure 8. Longitudinal sections of the spectral cones of the incident, reflected and transmitted fields. The surface of discontinuity between the two media is situated at the $z = 0$ plane.

These values are then used to estimate the deviation of the square root appearing in $\tilde{\gamma}_z(\phi)$ from the $\gamma_z(\phi)(c_1/c_2)$ term associated with a rotated z variable appearing in an exact X-wave tilted in the second medium at an angle α_2 and characterized by the angle ξ_2 . The resulting deviation $\Delta(\phi)$ is equal to

$$\begin{aligned} \Delta(\phi) &= \tilde{\gamma}(z) - (c_1/c_2)\gamma(z) \\ &= \sqrt{(c_1/c_2)^2 - 1 + (\sin \xi_1 \sin \alpha_1 \sin \phi + \cos \xi_1 \cos \alpha_1)^2} \\ &\quad - (c_1/c_2) (\sin \xi_2 \sin \alpha_2 \sin \phi + \cos \xi_2 \cos \alpha_2). \end{aligned} \tag{36}$$

For short distances from the interface, the condition $z\Delta(\phi) \ll a$ is satisfied for all values of $\Delta(\phi)$. Hence, the transmitted field remains localized until it reaches the dispersion limit

$$z_d = \frac{a}{|\overline{\Delta}(\phi)|}. \tag{37}$$

Here, $\overline{\Delta}(\phi)$ is the average deviation over the range $0 \leq \phi < 2\pi$.

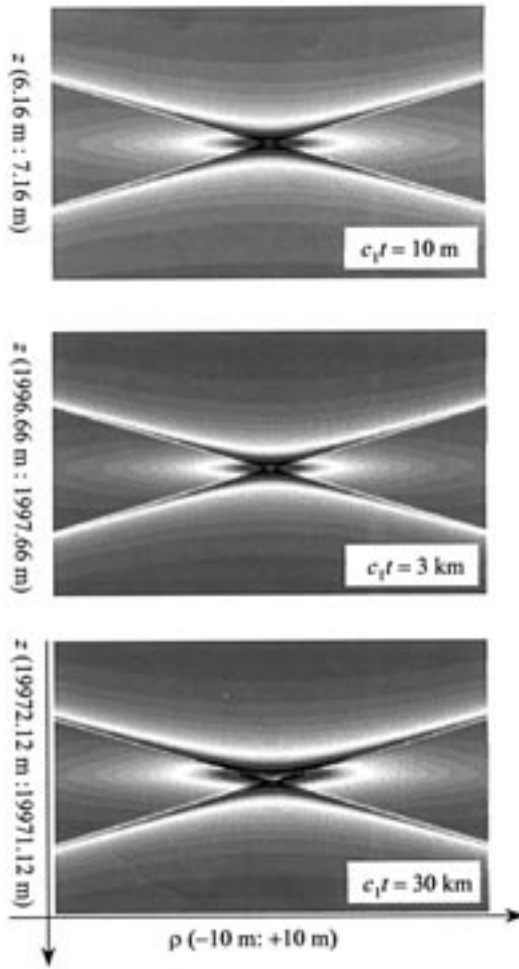
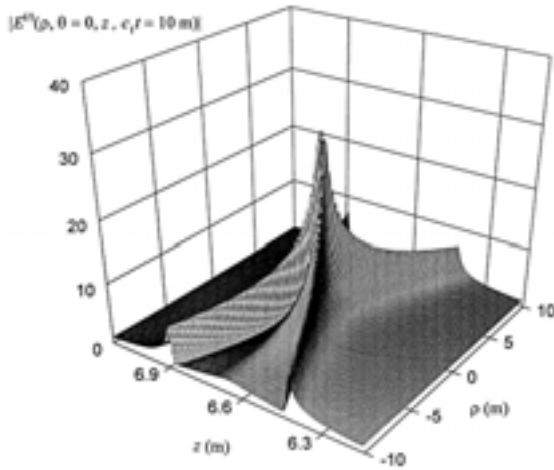
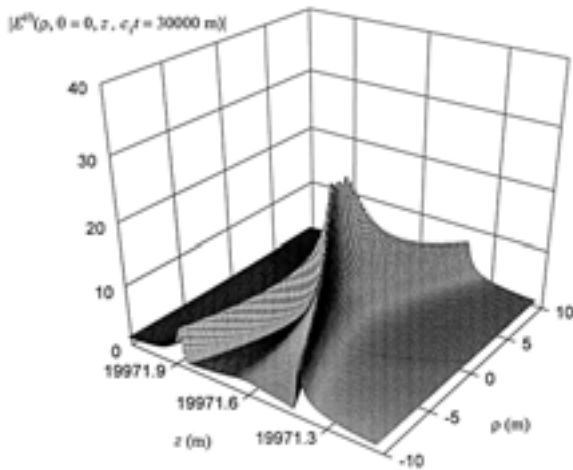


Figure 9. Density plot showing a time sequence of the transmitted field due to the X-wave shown in Fig. 1. The dielectric medium is chosen such that $(c_1/c_2) = 1.5$ and the angle of inclination of the incident field $\alpha_1 = 5^\circ$. The pulse does not disperse for several kilometers from the interface.

In Fig. 9, we present density plots of the transmitted field at $c_1t = 10$, 3000 and 30000 m. The incident X-wave has the same characteristics as the one displayed in Fig. 1. It is clear that the transmitted pulse stays localized for a long distance and starts to disperse at $c_1t = 30000$ m. The surface plots provided in Fig. 10 show that the



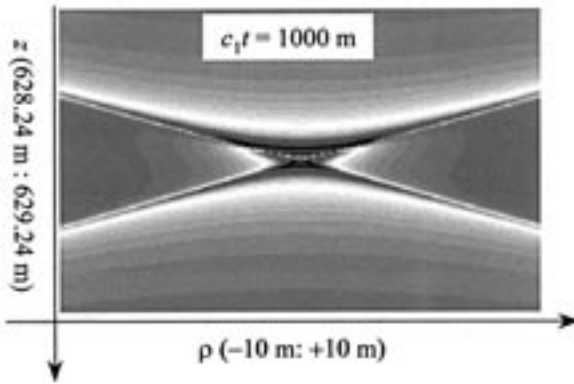
(a)



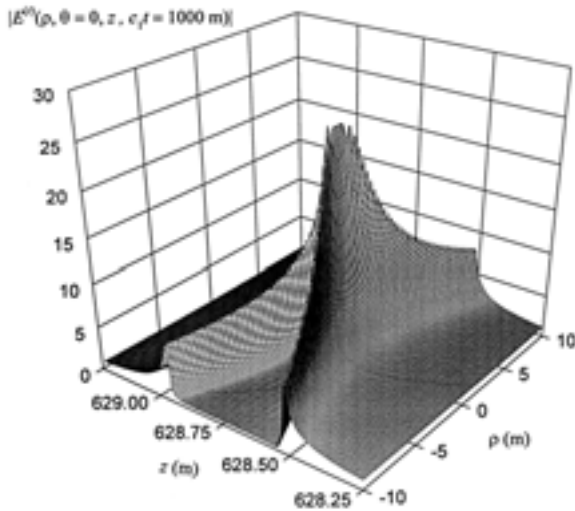
(b)

Figure 10. Surface plots of the transmitted field evaluated at (a) $c_1 t = 10$ m and (b) $c_1 t = 30$ km.

pulse stays localized for distances of order of 10 km. Even after 10 km, the dispersion of the pulse is very slow because of the small angle of incidence α_1 . To demonstrate the effect of increasing α_1 , in Fig. 11a we provide a density plot of the transmitted field for $\alpha_1 = 30^\circ$ at $c_1 t = 1000$ m. In Fig. 11b, we display a surface plot of the same



(a)



(b)

Figure 11. Magnitude of the transmitted electric field evaluated at $c_1 t = 1000$ m. The transmitted field is due to an X-wave incident at $\alpha_1 = 30^\circ$ and having $a = 0.01$ m and $\xi_1 = 2^\circ$. (a) Density plot and (b) 3-D surface plot.

field. The two figures show that the transmitted field starts to disperse at $z = 600$ m. Another factor that affects the dispersion of the transmitted pulse is the parameter a that controls the axial and lateral widths of the pulse and its frequency bandwidth [8]. The expression

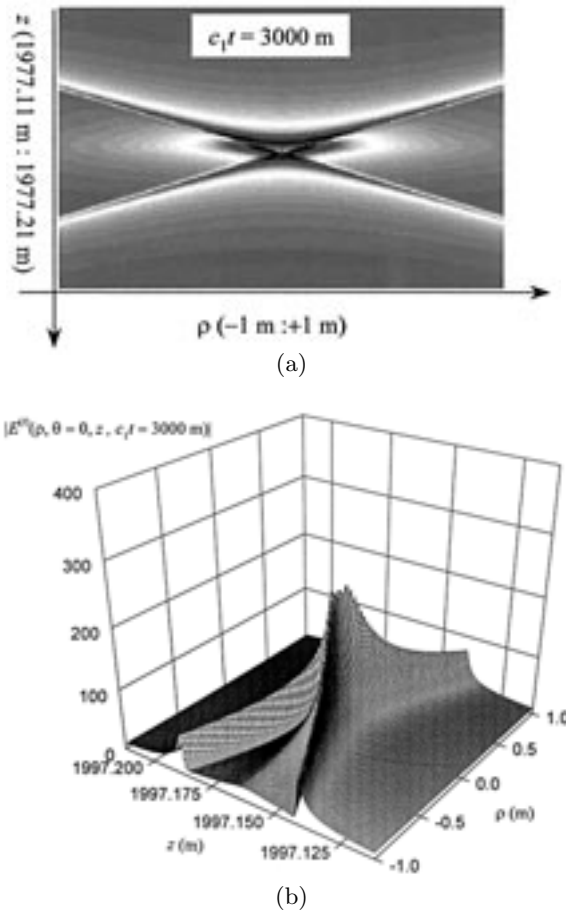


Figure 12. Magnitude of the transmitted electric field evaluated at $c_1t = 3000$ m. The transmitted field is due to an X-wave incident at $\alpha_1 = 5^\circ$ and having $a = 0.01$ m and $\xi_1 = 8^\circ$. (a) Density plot and (b) 3-D surface plot.

given in Eq. (37) indicates that the dispersion limit decreases as the parameter a becomes smaller. The density plot in Fig. 12 supports this conclusion showing that reducing a to 0.001 m causes the pulse to disperse at $c_1t = 3000$ m. It is important to note that both the lateral and transverse widths of the pulse are reduced by a factor of ten when compared to the pulse shown in Fig. 10b. The third factor that affects the dispersion rate of the transmitted field is the axicon angle ξ_1 . In Fig. 13, we display the transmitted field resulting from an

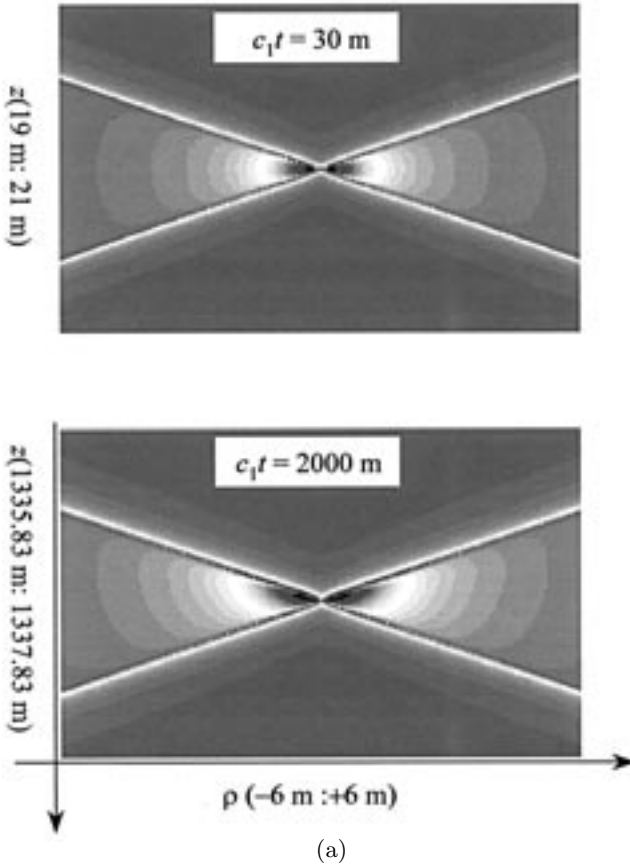
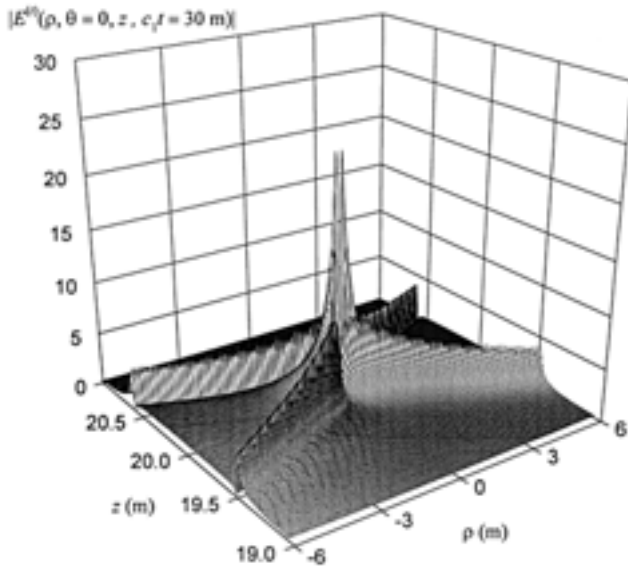
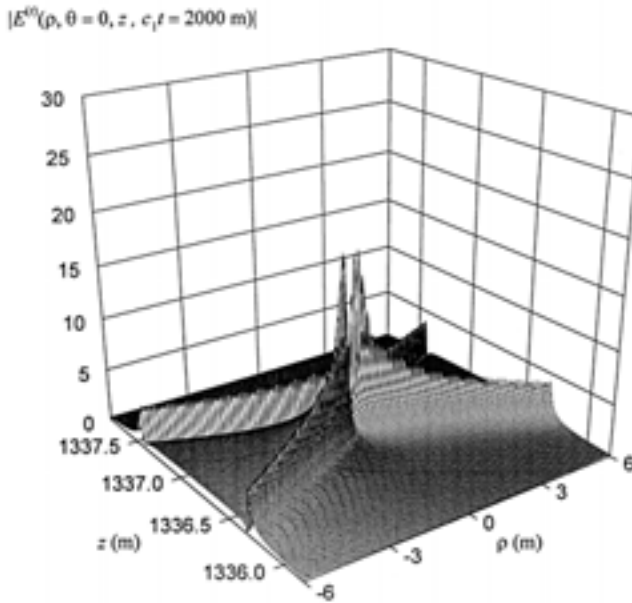


Figure 13. Magnitude of the transmitted electric field due to an X-wave incident at $\alpha_1 = 5^\circ$. The incident X-wave has $a = 0.001$ m and $\xi_1 = 2^\circ$. (a) Density plot for $c_1t = 30$ m and $c_1t = 2000$ m, (b) 3-D surface plot for $c_1t = 30$ m and (c) 3-D surface plot for $c_1t = 2000$ m.

incident X-wave having $\xi_1 = 8^\circ$. Plots for $c_1t = 30$ and 2000 m are provided. The figures show that dispersion becomes visible at a distance of 1336 m from the interface. Therefore, an increase in ξ_1 causes the transmitted field to disperse at shorter distances. Table 1 displays values of z_d calculated for the different parameter choices used in Figs. 10–13. The calculated z_d values are approximately half the distances used in the figures. We did not provide plots of the transmitted fields at the respective z_d distances because at those positions the pulses are still localized. At z_d , dispersion starts becoming effective but is



(b)



(c)

Figure 13. Continued.

not yet observable. The figures are plotted at approximately twice z_d to clearly show the dispersion of the transmitted field. Comparing the values of z_d in Table 1 to the decay of the pulses plotted in Figs. 10–13, we can conclude that the dispersion distance given in Eq. (37) characterizes accurately the decay of the transmitted field.

Table 1.

ξ_1	α_1	(c_1/c_2)	a (m)	z_d (m)
2°	5°	1.5	0.01	11600
2°	30°	1.5	0.01	297
2°	5°	1.5	0.001	1160
8°	5°	1.5	0.01	720

4. CONCLUSION

In this work, we have considered the reflection and transmission of electromagnetic X-waves obliquely incident on a planar air-dielectric interface. The analysis adopted has been based on a spectral decomposition of the incident pulse into plane wave components specified by wave vectors forming a conical surface. The boundary conditions at the interface are satisfied by the individual plane waves that are represented in the form of an angular integration (synthesis) of azimuthally dependent pulses. It has been shown that the incident and azimuthally dependent pulses travel at the same speed and, consequently, add up coherently at any observation point to form a LW pulse. In contradistinction, the azimuthally dependent pulses associated with the transmitted field travel at different speeds, thus causing the dispersion of transmitted field. It has been shown that the localization range of the transmitted field depends on the temporal frequency bandwidth, the angle of inclination and the axicon angle of the incident X-wave pulse. For normal incidence, the transmitted field retain its LW structure. These results are in agreement with the geometric approach inferred from the pulsed plane wave representation introduced in Ref. 17.

In previous investigations, the transmitted field has been shown to lose the LW structure of the incident pulse [14, 15]. This may give the wrong impression that the transmitted field is not localized at all. The present work demonstrates that the transmitted field stays localized up to a distance that depends on the characteristics of the

incident field. Furthermore, the analysis reveals that the transmitted LW structure resulting from normal incidence changes continuously into a progressively degenerate structure as the angle of incidence is increased. This information is essential for practical applications that make use of the localized character of the transmitted field, e.g., in detection and identification of buried objects. The information should be used in conjunction with the fact that finite-energy LWs have a finite range of localization [8, 23, 24]. Thus, one should always be able to determine which effect dominates in causing the decay of the transmitted field; the diffraction effect due to the initial finite size of the source or the dispersion effects described in this paper. Such an assessment can be effected by comparing the estimate for the range of localization z_d given in Eq. (37) to formulas specifying the diffraction lengths of LWs [8, 23, 24].

In summary, in his paper we have described a spectral technique for evaluating the reflections and transmissions of electromagnetic X-waves incident on a planar air-dielectric interface. We have provided a full wave explanation of the dispersion of the transmitted fields. The adopted analysis yields an estimate for the dispersion rate. Furthermore, it demonstrates the effects of polarization on the shaping of the transmitted and reflected pulses. We would like to point out that our investigation is not exhaustive. Some generalizations, e.g., the incorporation of multi-layered geometries and the possible identification of the dielectric characteristics of the different layers, are discussed in Ref. 17. Further extensions are required when we take into consideration loss and dispersion mechanisms of the second medium. In addition, special attention should be given to the incorporation of evanescent fields when incidence takes place from an optically slower medium to a faster one. For acoustic X-waves, it has been shown that at near-critical incidence the transmitted field becomes highly focused at short distances from the interface [16].

APPENDIX A

The wave vectors associated with the spectral wave components of a normally incident X-wave lie on a conical surface as shown in Fig. 1 of Ref. 17. The unit vector \vec{s} defines the polarization of each plane wave component. For a normally incident X-wave, we choose $\vec{s} = \hat{u}_\phi$. Superposition over such plane wave components gives an azimuthally symmetric wave with E_ϕ , H_ρ , and H_z electromagnetic components.

For normal incidence, the wave vectors are defined as

$$\vec{k} = k_x \vec{u}_x + k_y \vec{u}_y + k_z \vec{u}_z. \quad (\text{A1})$$

The polarization vector associated with each wave vector is given by

$$\vec{s} = -(k_y/\chi) \vec{u}_x + (k_x/\chi) \vec{u}_y. \quad (\text{A2})$$

For oblique incidence, the spectral cone is rotated around the X-axis through angle α_1 . The wave vectors associated with the spectral plane wave components are transformed so that $\vec{k}' = M^T \vec{k}$. Specifically, we get,

$$\vec{k}' = k_x \vec{u}_x + (k_y \cos \alpha_1 - k_z \sin \alpha_1) \vec{u}_y + (k_y \sin \alpha_1 + k_z \cos \alpha_1) \vec{u}_z. \quad (\text{A3})$$

To preserve the TE character of the incident field, the vector \vec{s} is also rotated using the transformation $\vec{s}' = M^T \vec{s}$. This gives rise to the following explicit expression for the polarization vector:

$$\vec{s}' = -(k_y/\chi) \vec{u}_x + (k_x/\chi) \cos \alpha_1 \vec{u}_y + (k_x/\chi) \sin \alpha_1 \vec{u}_z. \quad (\text{A4})$$

When the spectral cone is rotated, the polarization vector \vec{s}' acquires both parallel and normal components with respect to the plane of incidence. Our aim in this appendix is to identify explicitly these components and, hence, to use this information in calculating the reflected and transmitted fields. The reflected and transmitted fields are calculated by carrying out Fourier integrations over \vec{k}' . As a consequence, we need to recalculate \vec{s}'_{\perp} and \vec{s}'_{\parallel} in terms of the components of \vec{k}' . The polarization unit vector given in Eq. (A4) can be rewritten in terms of (k'_x, k'_y, k'_z) after substituting $k_x = k'_x$ and $k_y = k'_y \cos \alpha_1 + k'_z \sin \alpha_1$. This substitution yields

$$\begin{aligned} \vec{s}' = & -((k'_y/\chi') \cos \alpha_1 + (k'_z/\chi') \sin \alpha_1) \vec{u}_x + (k'_x/\chi') \cos \alpha_1 \vec{u}_y \\ & + (k'_x/\chi') \sin \alpha_1 \vec{u}_z, \end{aligned} \quad (\text{A5})$$

where $\chi' = (k_x'^2 + (k'_y \cos \alpha_1 + k'_z \sin \alpha_1)^2)^{1/2}$. The components of \vec{s}' along the z -axis and in the xy -plane are obtained from Eq. (A5); specifically,

$$\vec{s}'_z = (k'_x/\chi') \sin \alpha_1 \vec{u}_z, \quad (\text{A6})$$

$$\vec{s}'_{xy} = -((k'_y/\chi') \cos \alpha_1 + ((k'_z/\chi') \sin \alpha_1) \vec{u}_x + ((k'_x/\chi') \cos \alpha_1 \vec{u}_y. \quad (\text{A7})$$

The plane of incidence is defined as the plane containing the two vectors \vec{k}' and \vec{u}_z . Hence, the condition $\vec{s}'_{\perp} \cdot \vec{k}' = 0$ should be satisfied, where

$$\vec{s}'_{\perp} = Q_1 \vec{u}_x + Q_2 \vec{u}_y.$$

This is equivalent to the constraint

$$Q_1 = -Q_2 (k'_y/k'_x).$$

The vector \vec{s}'_{\perp} can then be written as

$$\vec{s}'_{\perp} = (Q/\chi') \{-k'_y \vec{u}_x + k'_x \vec{u}_y\}. \quad (\text{A8})$$

The parallel part of \vec{s}' equals the difference between \vec{s}'_{xy} and \vec{s}'_{\perp} added to \vec{s}'_z . Specifically,

$$\begin{aligned} \vec{s}'_{\parallel} = & -(1/\chi') [(k'_y \cos \alpha_1 + k'_z \sin \alpha_1 - Qk'_y) \vec{u}_x \\ & - (k'_x \cos \alpha_1 - Qk'_x) \vec{u}_y - k'_x \sin \alpha_1 \vec{u}_z]. \end{aligned} \quad (\text{A9})$$

The constant Q can be determined from the normalization condition, $|\vec{s}'_{\parallel}|^2 + |\vec{s}'_{\perp}|^2 = 1$. After some manipulations, we solve for the parameter Q , to obtain

$$Q = \frac{k'_y (k'_y \cos \alpha_1 + k'_z \sin \alpha_1) + k'_x{}^2 \cos \alpha_1}{(k'_y{}^2 + k'_x{}^2)}. \quad (\text{A10})$$

The components of \vec{s}' normal and parallel to the plane of incidence can be written explicitly as

$$\vec{s}'_{\perp} = \frac{k'_y (k'_y \cos \alpha_1 + k'_z \sin \alpha_1) + k'_x{}^2 \cos \alpha_1}{(k'_x{}^2 + k'_y{}^2) \sqrt{k'_x{}^2 + (k'_y \cos \alpha_1 + k'_z \sin \alpha_1)^2}} \{-k'_y \vec{u}_x + k'_x \vec{u}_y\}. \quad (\text{A11})$$

$$\vec{s}'_{\parallel} = \frac{k'_x \sin \alpha_1}{\sqrt{k'_x{}^2 + (k'_y \cos \alpha_1 + k'_z \sin \alpha_1)^2}} \left\{ \frac{-k'_z}{(k'_x{}^2 + k'_y{}^2)} (k'_x \vec{u}_x + k'_y \vec{u}_y) + \vec{u}_z \right\}. \quad (\text{A12})$$

APPENDIX B

Our aim in this appendix is to determine the components of the wave vector \vec{k} associated with the spectral components of the reflected and

transmitted X-wave fields. We assume that the surface of discontinuity between the two media lies on the $z = 0$ plane. An X-wave is incident from the negative z -hemisphere to the positive one along a propagation axis lying in the $x = 0$ plane and titled at an angle α_1 with the z -axis. To determine the form of the reflected and transmitted wave vectors, we apply the following rules to their components:

- (1) $k_{xref} = k_{xinc}$, $k_{yref} = k_{yinc}$ and $k_{zref} = -k_{zinc}$.
- (2) $k_{xtrans} = k_{xinc}$, $k_{ytrans} = k_{yinc}$ and k_{ztrans} to be determined using Snell's law $\sin \theta_{k2} = (c_2/c_1) \sin \theta_{k1}$.

For an obliquely incident field, the wave vector is given by $\vec{k}_{inc} = (\omega/c_1)\vec{\gamma}_i$, where $\vec{\gamma}_i$ is a unit vector with components

$$\gamma_{ix} = \sin \theta_{k1} \cos \phi_{k1} = \sin \xi_1 \cos \phi. \quad (\text{B1})$$

$$\gamma_{iy} = \sin \theta_{k1} \sin \phi_{k1} = \sin \xi_1 \sin \phi \cos \alpha_1 - \cos \xi_1 \sin \alpha_1. \quad (\text{B2})$$

$$\gamma_{iz} = \cos \theta_{k1} = \sin \xi_1 \sin \phi \sin \alpha_1 + \cos \xi_1 \cos \alpha. \quad (\text{B3})$$

These three relations are parametric equations describing the components of a unit vector lying on a circular conic surface having an apex angle ξ_1 and rotated around the x -axis through an angle α_1 . It will be seen that the angular dependence of the components of the unit vectors associated with the reflected and transmitted fields is analogous to that given in Eqs. (B1–3). In the sequel, we shall use the simpler notation $\gamma_x = \gamma_{ix}$, $\gamma_y = \gamma_{iy}$ and $\gamma_z = \gamma_{iz}$.

According to rule (1), the reflected wave vector can be written as $\vec{k}_{ref} = (\omega/c_1)\vec{\gamma}_r$, with the components of the unit vector $\vec{\gamma}_r$ given by

$$\gamma_{rx} = \gamma_x = \sin \xi_1 \cos \phi. \quad (\text{B4})$$

$$\gamma_{ry} = \gamma_y = \sin \xi_1 \sin \phi \cos \alpha_1 - \cos \xi_1 \sin \alpha_1. \quad (\text{B5})$$

$$\gamma_{rz} = -\gamma_z = -(\sin \xi_1 \sin \phi \sin \alpha_1 + \cos \xi_1 \cos \alpha_1). \quad (\text{B6})$$

These components define a circular cone similar to that of the incident cone, but rotated through an angle $(\pi - \alpha_1)$ and with the replacement $\phi \rightarrow -\phi$. The second condition is necessary for the incident and reflected wave vectors to satisfy the relation $\theta_{k1} = \theta_{k2}$ in their plane of incidence.

As for the transmitted wave vector, we have $\vec{k}_{trans} = (\omega/c_1)\vec{\gamma}_t$, where

$$\gamma_{tx} = \gamma_x = \sin \xi_1 \cos \phi, \quad (\text{B7})$$

$$\gamma_{ty} = \gamma_y = (\sin \xi_1 \sin \phi \cos \alpha_1 - \cos \xi_1 \sin \alpha_1). \quad (\text{B8})$$

The z -component of the transmitted wave vector is given as

$$k_{ztrans} = (\omega/c_2) \cos \theta_{k2}. \quad (\text{B9})$$

Notice that the dispersion relationship in the second medium is satisfied because

$$\begin{aligned} k_{xtrans} &= (\omega/c_2) \sin \theta_{k2} \cos \phi_{k2} = (\omega/c_1) \sin \theta_{k1} \cos \theta_{k1}, \\ k_{ytrans} &= (\omega/c_2) \sin \theta_{k2} \sin \phi_{k2} = (\omega/c_1) \sin \theta_{k1} \sin \theta_{k1}, \\ \sqrt{k_{xtrans}^2 + k_{ytrans}^2} &= (\omega/c_2) \sin \theta_{k2} = (\omega/c_1) \sin \theta_{k1}, \end{aligned} \quad (\text{B10})$$

which is Snell's law. It, then, follows that

$$k_{xtrans}^2 + k_{ytrans}^2 + k_{ztrans}^2 = (\omega/c_2)^2 (\sin^2 \theta_{k2} + \cos^2 \theta_{k2}) = (\omega/c_2)^2. \quad (\text{B11})$$

This is the correct dispersion relationship for waves propagating in the second medium. The z -component of the transmitted wave vector given in Eq. (B9) can be rewritten as follows:

$$k_{ztrans} = (\omega/c_2) \sqrt{1 - \sin^2 \theta_{k2}}.$$

Using Snell's law, we obtain

$$\begin{aligned} k_{ztrans} &= (\omega/c_2) \sqrt{1 - (c_2/c_1)^2 \sin^2 \theta_{k1}} \\ &= (\omega/c_2) \sqrt{1 - (c_2/c_1)^2 + (c_2/c_1)^2 \cos^2 \theta_{k1}}. \end{aligned}$$

Substituting for $\cos \theta_{k1}$ in terms of ξ_1 , α_1 and ϕ , we get

$$\begin{aligned} k_{ztrans} &= (\omega/c_1)(c_1/c_2) \\ &\cdot \sqrt{1 - (c_2/c_1)^2 + (c_2/c_1)^2 (\sin \xi_1 \sin \phi \sin \alpha_1 + \cos \xi_1 \cos \alpha_1)^2}. \end{aligned}$$

Therefore, the z -component of the transmitted unit vector $\vec{\gamma}_t$ is given by

$$\begin{aligned} \gamma_{tz} &= \tilde{\gamma}_z = (c_1/c_2) \\ &\cdot \sqrt{1 - (c_2/c_1)^2 + (c_2/c_1)^2 (\sin \xi_1 \sin \phi \sin \alpha_1 + \cos \xi_1 \cos \alpha_1)^2}. \end{aligned} \quad (\text{B12})$$

REFERENCES

1. Brittingham, J. N., "Focus wave modes in homogeneous Maxwell equations: Transverse electric mode," *J. Appl. Phys.*, Vol. 54, 1179–1189, 1983.
2. Ziolkowski, R. W., "Exact solutions of the wave equation with complex source locations," *J. Math. Phys.*, Vol. 26, 861–863, 1985.
3. Besieris, I. M., A. M. Shaarawi, and R. W. Ziolkowski, "A bidirectional traveling plane wave representation of exact solutions of the scalar wave equation," *J. Math. Phys.*, Vol. 30, 1254–1269, 1989.
4. Lu, J. Y. and J. F. Greenleaf, "Nondiffracting X waves — exact solutions to free space scalar wave equation and their finite aperture realization," *IEEE Trans. Ultrason. Ferroelec. Freq. Contr.*, Vol. 39, 19–31, 1992.
5. Ziolkowski, R. W., I. M. Besieris, and A. M. Shaarawi, "Aperture realizations of the exact solutions to homogeneous-wave equations," *J. Opt. Soc. Am. A*, Vol. 10, 75–87, 1993.
6. Recami, E., "On the localized 'X-shaped' superluminal solutions to Maxwell's equations," *Physica A*, Vol. 252, 586–610, 1998.
7. Besieris, I., M. Abdel-Rahman, A. Shaarawi, and A. Chatzipetros, "Two fundamental representations of localized pulse solutions of the scalar wave equation," *Progress in Electromagnetics Research (PIER)* 19, 1–48, 1998.
8. Shaarawi, A. M., "Comparison of two localized wavefields generated from dynamic apertures," *J. Opt. Soc. Am. A*, Vol. 14, 1804–1816, 1997.
9. Ziolkowski, R. W., D. K. Lewis, and B. D. Cook, "Experimental verification of the localized wave transmission effect," *Phys. Rev. Lett.*, Vol. 62, 147–150, 1989.
10. Lu, J. Y. and J. F. Greenleaf, "Experimental verification of nondiffracting X waves," *IEEE Trans. Ultrason. Ferroelec. Freq. Contr.*, Vol. 39, 441–446, 1992.
11. Saari, P. and K. Reivelt, "Evidence of X-shaped propagation-invariant localized light waves," *Phys. Rev. Lett.*, Vol. 21, 4135–4138, 1997.
12. Power, D., R. Donnelly, and R. MacIsaac, "Spherical scattering of superpositions of localized waves," *Phys. Rev. E*, Vol. 48, 1410–1417, 1993.
13. Lu, J. Y., M. Fatemi, and J. F. Greenleaf, "Pulsed-echo imaging with X wave," *Acoust. Imag.*, P. Tortoli and L. Masotti (Eds.), Vol. 22, 191–196, 1996.
14. Hillion, P., "How do focus wave modes propagate across a discontinuity in a medium?" *Optik* Vol. 93, 67–72, 1993.

15. Donnelly, R. and D. Power, "The behavior of electromagnetic localized waves at a planar interface," *IEEE Trans. Antennas Propagat.*, Vol. 45, 580–591, 1997.
16. Shaarawi, A. M., I. M. Besieris, A. M. Attiya, and E. El-Diwany, "Acoustic X-wave reflection and transmission at a planar interface: spectral analysis," *J. Acoust. Soc. Am.*, Vol. 107, 70–86, 2000.
17. Attiya, A. M., E. El-Diwany, A. M. Shaarawi, and I. M. Besieris, "Reflection and transmission of electromagnetic X-waves in the presence of planarly layered media: The pulsed plane wave representation," submitted to *J. Electromagn. Waves Appl.*.
18. Fagerholm, J., A. T. Friberg, J. Huttunen, D. P. Morgan, and M. M. Salomaa, "Angular-spectrum representation of non-diffracting X waves," *Phys. Rev. E*, Vol. 54, 4347–4352, 1996.
19. Friberg, A. T., J. Fagerholm, and M. M. Salomaa, "Space-frequency analysis of nondiffracting pulses," *Opt. Comm.*, Vol. 136, 207–212, 1997.
20. Shaarawi, A. M., R. W. Ziolkowski, and I. M. Besieris, "On the evanescent fields and the causality of the focus wave modes," *J. Math. Phys.*, Vol. 36, 5565–5587, 1995.
21. Shaarawi, A. M., I. M. Besieris, R. W. Ziolkowski, and S. M. Sedky, "Generation of approximate focus wave mode pulses from wide-band dynamic Gaussian aperture," *J. Opt. Soc. Am. A*, Vol. 12, 1954–1964, 1995.
22. Born, M. and E. Wolf, *Principles of Optics*, Pergamon Press, Oxford, 1989.
23. Hafizi, B. and P. Sprangle, "Diffraction effects in directed radiation beams," *J. Opt. Soc. Am. A*, Vol. 8, 705–717, 1991.
24. Sedky, S. M., A. M. Shaarawi, F. M. Taiel, and I. M. Besieris, "On the diffraction length of localized waves generated by dynamic apertures," *J. Opt. Soc. Am. A*, Vol. 13, 1719–1727, 1996.